nature biomedical engineering

Article

https://doi.org/10.1038/s41551-025-01424-6

LbuCas13a directly targets DNA and elicits strong *trans*-cleavage activity

Received: 2 February 2024

Accepted: 9 May 2025

Published online: 20 June 2025

Check for updates

Xiaolong Wu[1,3], Siyuan Luo[1,3], Chuanghao Guo[1], Yi Zhao[1], Jialing Zhong[1], Ronghuan Hu[1], Xinyao Yang[1], Conghui Liu[1], Qianling Zhang[2], Songkuan Zhuang[1], Yong Chen[1,2] ✉, Yizhen Liu[1] ✉ & Xueji Zhang[1] ✉

Traditionally perceived as an RNA-specific nuclease, Cas13a has been used primarily for RNA detection. We discover the ability of *Leptotrichia buccalis* Cas13a (LbuCas13a) to directly target DNA without the restrictions of protospacer flanking sequence and protospacer adjacent motif sequences, coupled with robust *trans*-cleavage activity. Contrary to conventional understanding, LbuCas13a does not degrade DNA targets. Our study reveals an enhancement in the single-nucleotide specificity of LbuCas13a against DNA compared to RNA. This heightened specificity is attributed to the lower affinity of CRISPR RNA (crRNA) towards DNA, raising the crRNA–DNA binding energy barrier. We introduce a molecular diagnostic platform called superior universal rapid enhanced specificity test with LbuCas13a (SUREST) for high-resolution genotyping. SUREST is capable of detecting DNA concentrations of CYP2C19 (rs4986893) as minute as 0.3 aM (0.18 cps μl^{-1}). We also apply SUREST to human genotyping scenarios, indicating that SUREST performs well across a broad range of mutations and sequence contexts. SUREST represents an advancement in real-time nucleic acid detection, making it a useful tool for pathogen identification and mutation analysis in clinical diagnostics.

The realm of CRISPR and Cas systems[1,2] has been a beacon of innovation in gene editing and diagnostics, with Cas13a and Cas12a spearheading advancements because of their *trans*-cleavage activities[3,4]. Historically, these systems have been constrained to RNA or DNA substrates, with Cas13a predominantly recognized as an RNA-targeting nuclease[5] and Cas12a as a DNA-targeting[6] counterpart. This specialization has underpinned the development of CRISPR-based diagnostics (CRISPR-Dx), leveraging their sequence-specific nuclease activity. Notable platforms like SHERLOCK[7], HOLMES[8] and DETECTR[9] have harnessed these properties, offering rapid and highly sensitive detection of nucleic acids even at the attomolar (aM) level.

Notwithstanding these advancements, the specificity of CRISPR-Dx in single-nucleotide polymorphism (SNP) discrimination remains a scientific challenge. In the investigation of single-nucleotide specificity in Cas12a nucleases, the introduction of a protospacer adjacent motif (PAM) sequence into the target DNA through amplification is essential because of PAM sequence dependency. However, even in the presence of a suitable PAM sequence, it is often necessary to decrease the affinity between the mismatch target and CRISPR DNA (crRNA) to improve specificity by designing a 'suboptimal crRNA'. Efforts to refine this specificity often involve introducing 'synthetic mismatches'[10,11], such as the RatioCRISPR[12] and cARMS[13] platforms, yet this approach can be plagued by increased off-target effects and reduced reaction efficiency because of the low match between crRNA and target RNA. More importantly, determining the optimal placement of synthetic mismatches is not intuitive and requires experimental evaluation for

[1]Research Center for Nanosensor Molecular Diagnostic & Treatment Technology, Shenzhen Key Laboratory of Nano-Biosensing Technology, College of Chemistry and Environmental Engineering, Shenzhen University, Shenzhen, People's Republic of China. [2]Graphene Composite Research Center, College of Chemistry and Environmental Engineering, Shenzhen University, Shenzhen, People's Republic of China. [3]These authors contributed equally: Xiaolong Wu, Siyuan Luo. ✉e-mail: chenyong103199@szu.edu.cn; yzliu@szu.edu.cn; zhangxueji@szu.edu.cn

each crRNA–target pairing[14,15]. Alternative strategies, such as chemically modified crRNA[16], have been explored to enhance specificity, but chemically modified crRNA is hardly used in CRISPR-Dx because of its high cost. Other studies reported that hairpin crRNA[17,18] showed improved CRISPR–Cas specificity, but these fall short of meeting the stringent requirements for robust genotyping. On the other hand, Cas13a shows tolerance to single-nucleotide mismatches in most cases[7,19,20] and the crRNA–target RNA duplex structure is so stable[21] that a 'mismatch' is not enough to damage the stability between the RNA target and crRNA, resulting in Cas13a's very unstable performance in single-nucleotide-specific studies. We infer that a viable strategy to improve the specificity of the Cas13a system without extra design is to replace the RNA duplex with an RNA–DNA duplex to decrease the affinity between crRNA and its targets.

In this study, we demonstrate the ability of *Leptotrichia buccalis* Cas13a (LbuCas13a) to directly target DNA and elicit strong *trans*-cleavage activity. This finding sets LbuCas13a apart from its conventional role as an RNA-targeting nuclease. We find that the recognition target DNA of LbuCas13a is not affected by protospacer flanking sequence (PFS)[5] sequences (compared to the Cas13a–RNA system); even the restriction of PAM[22] sequences is not present in studies of single-nucleotide specificity compared to Cas12a–DNA. Targeting DNA with LbuCas13a demonstrated high single-nucleotide specificity without the need for synthetic mismatches. The results indicate that the LbuCas13a–DNA complex showcases a 19-fold increase in single-nucleotide specificity compared to its RNA-targeting counterpart. The main reason is that the affinity of crRNA to DNA is weaker than that of crRNA to RNA[23], which increases the reaction energy barrier for crRNA binding to its targets. LbuCas13a, functioning as an RNase, distinguishes itself by not causing damage to the target DNA.

Leveraging these insights, we propose the superior universal rapid enhanced specificity test with LbuCas13a (SUREST) platform. SUREST outperforms conventional CRISPR-Dx systems by offering single-nucleotide specificity and the capability of retesting without damaging the target nucleic acid. Compared with the traditional CRISPR-Dx system based on Cas13a, SUREST offers the advantage of detecting nucleic acids without the necessity of a redundant RNA target conversion process. Compared to the CRISPR-Dx system based on Cas12a, SUREST can specifically target DNA without the restrictions imposed by the PAM sequence. This platform holds potential in molecular diagnostics, particularly in pathogen detection and mutation analysis.

Result

DNA-targeting and *trans*-cleavage activity of LbuCas13a

Cas13a is traditionally recognized as an RNA-targeting ribonuclease. The standard LbuCas13a experimental process is shown in Fig. 1a. The crRNA was produced through in vitro T7 transcription and then bonded to LbuCas13a to initiate RNA targeting. Once the ternary complex had formed, the *trans*-cleavage activity was activated and started to digest the RNA reporter, which can generate a strong signal. At the same time, the RNA target would be cleaved by *cis*-cleavage activity. Upon meticulous investigation, we confirmed that LbuCas13a exhibits evident *trans*-cleavage activity on DNA (Fig. 1b and Supplementary Fig. 1). To be specific, our experimental design methodically omitted one of the four critical components (LbuCas13a, crRNA, reporter gene, synthetic DNA targets) at a time, confirming that the absence of any element led to assay failure. This substantiated that the potent *trans*-cleavage activity of LbuCas13a is DNA-activated.

Notably, the target DNA in our experiments lacked the typical PAM sequence (TTTN) associated with the Cas12a system, suggesting that the activation of the LbuCas13a–DNA system is not constrained by a specific PAM sequence. Furthermore, the gel imaging results revealed intact target DNA, indicating that the LbuCas13a nuclease does not cleave the DNA target through *cis*-cleavage (Supplementary Fig. 2).

Next, to confirm the nuclease substrate specificity of LbuCas13a activated by DNA, the RNA (6U) and DNA (6T) reporters were tested. As shown in Supplementary Fig. 3, a high signal was only observed by using RNA reporters, showing specificity towards RNA substrates, which is similar to previous research on LbuCas13a RNase structure domain specificity[24]. Our further experiment, recycling the original test sample to activate LbuCas13a, also confirmed this property (Supplementary Fig. 4). These characteristics stand in contrast to the standard Cas13a–RNA system.

The binding of single-stranded DNA (ssDNA) to Cas13a is due to the single-stranded binding interaction. However, the binding of Cas13a to double-stranded DNA (dsDNA) is very surprising given the absence of helicase domains in Cas13a and its known preference for single-stranded RNA other than dsRNA. To confirm the interaction between the LbuCas13a–crRNA complex and dsDNA, we designed a dsDNA probe, which labelled carboxyfluorescein (FAM) on the target strand and Black Hole Quencher (BHQ) on the non-target strand (Supplementary Fig. 5). As shown in Fig. 1c, a signal increase was observed when we added LbuCas13a and crRNA to the reaction containing the dsDNA probe, while there was a slight signal response when we added crRNA or water. This shows dsDNA unwinding under the help of the LbuCas13a–crRNA complex, which supports the activation of LbuCas13a by DNA. Also, we conducted an electrophoretic mobility shift assay (EMSA) with increasing concentrations of LbuCas13a–crRNA complexed ribonucleoprotein (RNP) and a fixed concentration of 25-nM non-target strand 5′ FAM-labelled dsDNA target. As expected, we observed a slow mobility species representing the dsDNA-bound LbuCas13a–crRNA complex when the RNP concentration increased to 12.5 nM (Fig. 1c). Notably, when the RNP concentration increased to 50 nM, we did not observe the dsDNA band, suggesting that all dsDNA substrates bound with RNP to formulate the LbuCas13a–crRNA–dsDNA complex. Next, we compared the capability for binding to dsDNA between LbuCas13a and *Lachnospiraceae* bacterium Cas12a (LbCas12a). The EMSA results suggest that LbuCas13a has a similar capability in targeting dsDNA with LbCas12a (Supplementary Fig. 6). These results demonstrate that LbuCas13a can be used as a DNA-binding module.

Furthermore, comparing several Cas13a variants, LbuCas13a emerged as the most effective in DNA-targeted *trans*-cleavage activity, as depicted in Supplementary Fig. 7. Moreover, to validate the reproducibility of LbuCas13a's activity across different sources, we compared proteins from several suppliers (Supplementary Fig. 8), observing only minor variations, thereby corroborating our findings. In our comparative analysis of LbuCas13a activated by DNA versus RNA, we noted that while both activations resulted in robust signal generation even at low concentrations (1 nM), there was a distinct difference in specificity (Fig. 1d and Supplementary Fig. 9). Particularly, LbuCas13a targeting DNA exhibited higher single-nucleotide specificity compared to RNA, with a distinguishing factor (DF) markedly higher for DNA. Specifically, when LbuCas13a targets RNA, both wild-type (WT) and single-nucleotide variant (SNV) targets generated a high signal, and the DF was nearly onefold; this is similar to a previous study[20]. However, dsDNA and ssDNA exhibited stronger single-nucleotide specificity; the DF was 12-fold and 98-fold, respectively. Notably, the signal strength of the RNA target ranked first, followed by dsDNA and ssDNA, while the single-nucleotide specificity was the opposite. This is because DNA–RNA strand affinity is weaker than RNA–RNA strand affinity[21,23], affecting signal strength and specificity.

Leveraging this specificity and efficiency, we developed SUREST for nucleic acid detection. To amplify the clinical diagnostic sensitivity, we integrated recombinase polymerase amplification (RPA) or PCR into SUREST, generating abundant ssDNA or dsDNA (Fig. 1b). The LbuCas13a RNP complex, upon encountering its DNA target, triggers the *trans*-cleavage of an RNA reporter, yielding a fluorescent signal. In summary, LbuCas13a, traditionally an RNA-targeting enzyme, now demonstrates DNA targeting. This opens avenues for its application

https://doi.org/10.1038/s41551-025-01424-6

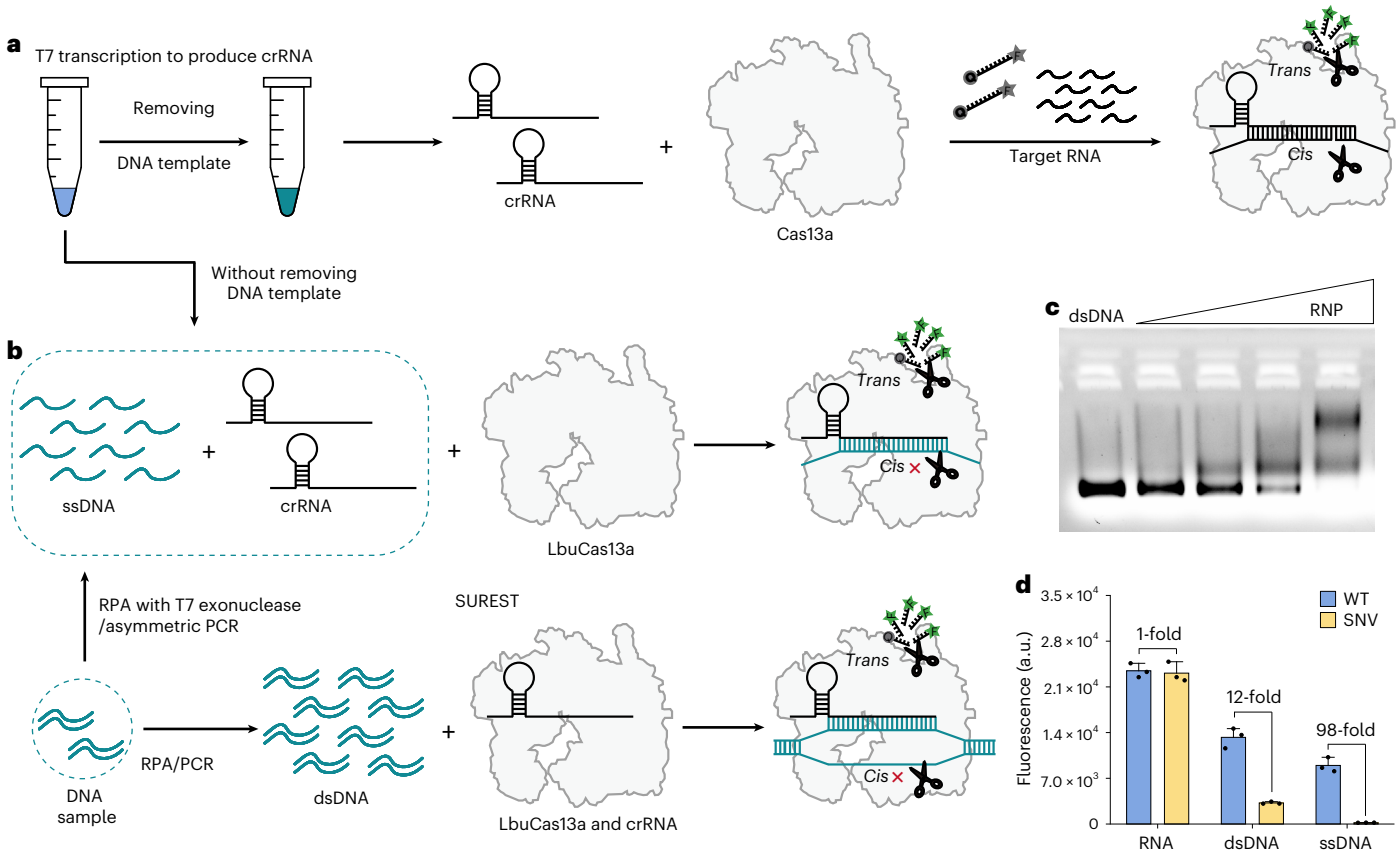

Fig. 1 | DNA-targeting and *trans*-cleavage activity of LbuCas13a. a, The conventional CRISPR-Dx framework using Cas13a for RNA targeting. **b**, The SURest system. **c**, Non-target strand 5′ FAM-labelled dsDNA EMSA with increasing concentrations of LbuCas13a–crRNA-complexed RNP. The dsDNA target concentration was 25 nM; the LbuCas13a concentration was 0, 62.5 nM, 125 nM, 250 nM and 500 nM for lanes 1–5, respectively; and the crRNA concentration was 0, 6.25 nM, 12.5 nM, 25 nM and 50 nM for lanes 1–5, respectively. **d**, Comparison of single-nucleotide specificity between RNA, dsDNA and ssDNA targets. The RNA target concentration was 100 pM while the dsDNA and ssDNA target concentration was 1 nM. $n = 3$ technical replicates; the bars represent the mean ± s.d. a.u., arbitrary unit.

in molecular diagnostics, with SURest exemplifying its potential to achieve high specificity and sensitivity in nucleic acid detection.

Influence of DNA sequence on LbuCas13a *trans*-cleavage

To determine the activation requirements of LbuCas13a for DNA targets, we conducted experiments with dsDNA and ssDNA targets of varying lengths complementary to the spacer region. Truncations from both the 5′ and 3′ ends of these targets were performed, with Fig. 2a illustrating the 5′ truncation scheme. Our initial findings with dsDNA targets (human papillomavirus type 16 (HPV16); Supplementary Table 4) showed no significant changes in fluorescence signals with 5′ end truncations until a 6-bp reduction, leading to a marked decrease in signal intensity (Fig. 2b). This trend was mirrored in ssDNA targets (Fig. 2c) and corroborated by kinetic analysis (Supplementary Fig. 10). Further tests using a different crRNA system (targeting the N gene of coronavirus disease 19 (COVID-19); Supplementary Tables 1 and 2) confirmed these observations (Supplementary Fig. 11). These results align with previous studies, suggesting that a minimum of 24 bp is necessary to effectively activate the *trans*-cleavage activity of LbuCas13a, as base pairs 25–28 are found outside the interaction channel with the LbuCas13a protein[25]. Truncations of 2–6 bp from the 3′ end (Fig. 2d) showed no increase in fluorescence with dsDNA targets (Fig. 2e), a finding that is consistent with ssDNA targets (Fig. 2f), as confirmed by kinetic curves (Supplementary Fig. 12). Interestingly, an overhang ssDNA (50 nt) accelerated the *trans*-cleavage activity of LbuCas13a (Supplementary Fig. 13), supporting the 'RESET' effect[26], which is beneficial in detection because of the long-chain nature of natural DNA and amplification products. These insights will inform the spacer region design in diagnostic systems using LbuCas13a for DNA targeting.

Furthermore, we examined if the *trans*-cleavage activity of LbuCas13a on DNA was influenced by the PFS. We designed four dsDNA (224 bp; Supplementary Table 4) and ssDNA (50 nt; Supplementary Table 2) targets with identical spacer complementary sequences but varying −1 sites (Fig. 2g). Our data indicated no significant PFS preference when targeting dsDNA, as signal generation was similar across A, T, C or G variations (Fig. 2h). This mirrors the behaviour of LbuCas13a with RNA targets[27,28]. While ssDNA targets showed similar trends (Fig. 2i), a slight delay was observed with G PFS, although not enough to affect detection. These findings are pivotal in guiding the design of LbuCas13a-based DNA-targeting diagnostic systems.

Detecting human parvovirus B19 with SURest

To optimize direct DNA detection using LbuCas13a on the SURest platform, we adjusted the reaction parameters. Initially, we evaluated the DNA-targeting signal response of LbuCas13a across a range of temperatures. As depicted in Fig. 3a, LbuCas13a exhibited peak activity at 33 °C, yielding the highest signal-to-noise ratio (SNR) of 256. Activity decreased at temperatures beyond this point, establishing 33 °C as the optimal temperature. Further evaluation across nine standard CRISPR–Cas buffers (Tolo Cas13a, NEBuffer 1.0, NEBuffer 2.0, NEBuffer 2.1, NEBuffer r1.1, NEBuffer r2.1, NEBuffer r3.1, NEBuffer r4.1 and Bio-Lifesci) identified the Bio-Lifesci buffer (no. 9) as providing the strongest fluorescence and highest SNR (196), as shown in Fig. 3b.

https://doi.org/10.1038/s41551-025-01424-6

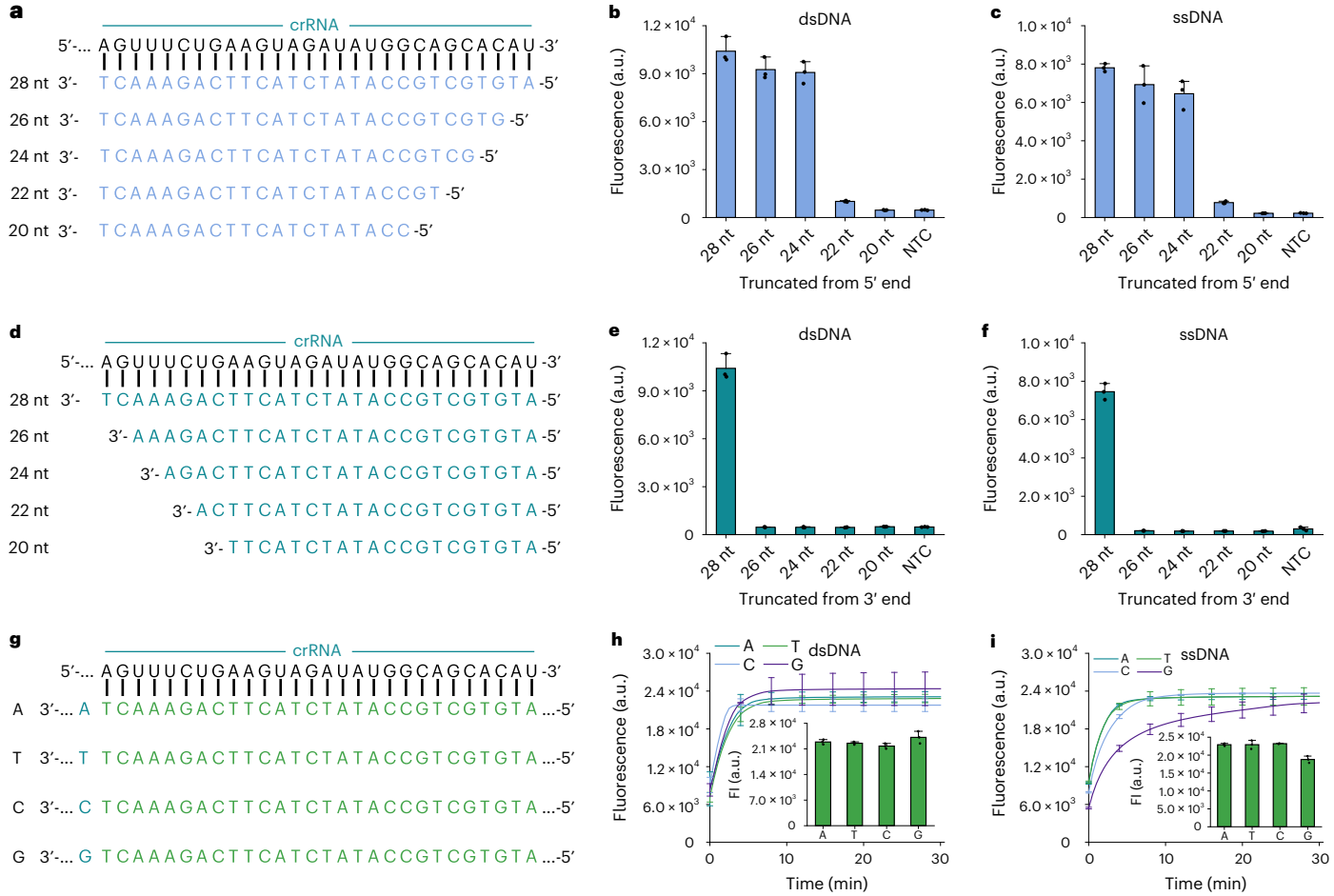

Fig. 2 | DNA sequence influence on *trans*-cleavage of LbuCas13a. a, Illustration of DNA target truncation from the 5′ end, showcasing crRNA (black) and the targeted DNA sequence (sky blue). **b**, Results from truncating the 5′ end of dsDNA. **c**, Results from truncating the 5′ end of ssDNA. **d**, Depiction of DNA target truncation from the 3′ end, with crRNA (black) and DNA target (cyan). **e**, Outcomes of truncating the 3′ end of dsDNA. **f**, Outcomes of truncating the 3′ end of ssDNA. **g**, Diagram for examining several PFS sequences, highlighting crRNA (black), DNA target (green) and PFS (cyan). **h**, Effects of different PFS sequences on LbuCas13a targeting dsDNA. **i**, Effects of different PFS sequences on LbuCas13a targeting ssDNA. **b**,**c**,**e**,**f**,**h**,**i**, The target concentration was 1 nM. $n = 3$ technical replicates; the bars represent the mean ± s.d. FI, fluorescence intensity.

Consequently, we determined 33 °C and Bio-Lifesci buffer (no. 9) as the optimal conditions for subsequent SURETS applications.

Next, we assessed the sensitivity of LbuCas13a using RNA, dsDNA and ssDNA substrates. LbuCas13a exhibited signal responses at 0.01 pM for RNA, 0.5 pM for dsDNA and 0.1 pM for ssDNA, respectively (Fig. 3c–e). Comparative analysis with LbCas12a, using ssDNA targets as shown in Supplementary Fig. 14, showed that LbCas12a exhibited a detectable signal response only at 1 pM, underscoring the sensitivity and signal strength of LbuCas13a. However, in real detection, we often introduce nucleic acid amplification systems such as RPA and loop-mediated isothermal amplification to achieve aM-level molecular detection. Therefore, SURETS can achieve comparative sensitivity with other CRISPR-Dx systems, such as SHERLOCK.

Given the performance in DNA detection, we applied SURETS to detect human parvovirus B19 (B19)[29], an ssDNA virus implicated in several diseases, including chronic anaemia. Supplementary Fig. 15 confirms the successful detection of a 1-nM B19 mimic using a specially designed crRNA targeting a 50-nt DNA fragment derived from B19 (Supplementary Table 2). We then developed a lateral flow readout assay for point-of-care testing (POCT) using FAM-biotin reporter cleavage. As shown in Fig. 3f,g, the accumulation of reporters at the streptavidin line on the strip inhibited the binding of the anti-FAM antibody gold nanoparticle conjugates to the protein on the antibody capture line; cleavage of the reporter reduced accumulation at the first line and resulted in a signal on the second line. This assay enabled naked-eye detection within 35 min (30 min for the CRISPR–Cas13a reaction and 5 min for the lateral flow readout), as demonstrated with a 1-nM B19 mimic in Fig. 3h. Sensitivity tests, illustrated in Supplementary Fig. 16, further confirmed the capacity of the lateral flow readout assay to detect B19 mimics at concentrations as low as 10 pM. These results demonstrate the robustness and sensitivity of the SURETS-based lateral flow readout for rapid, amplification-free and equipment-free detection of viruses[14,30–33].

SURETS for rapid HPV and hepatitis B virus detection

To validate the virus detection capability of SURETS, we targeted HPV16. HPV16 is a high-risk type of HPV infection associated with genital cancers and cervical cancer epithelial lesions[34]. By targeting dsDNA and integrating RPA, we established a rapid and sensitive detection platform, as shown in Fig. 4a. The results in Supplementary Fig. 17 demonstrate that the *trans*-cleavage activity of LbuCas13a can be activated using a synthetic HPV16 gene constructed on a pUC57-Simple plasmid (Supplementary Table 3). The integrated system, combining the RPA amplification and CRISPR–Cas13a reaction, reduced detection time to 21 min (15 min for RPA, 1 min for heating and 5 min for the CRISPR–Cas13a reaction), effectively detecting HPV16 targets as low as 1 aM (0.6 copies μl^{-1}), as demonstrated in Fig. 4b. Compared to SHERLOCK,

https://doi.org/10.1038/s41551-025-01424-6

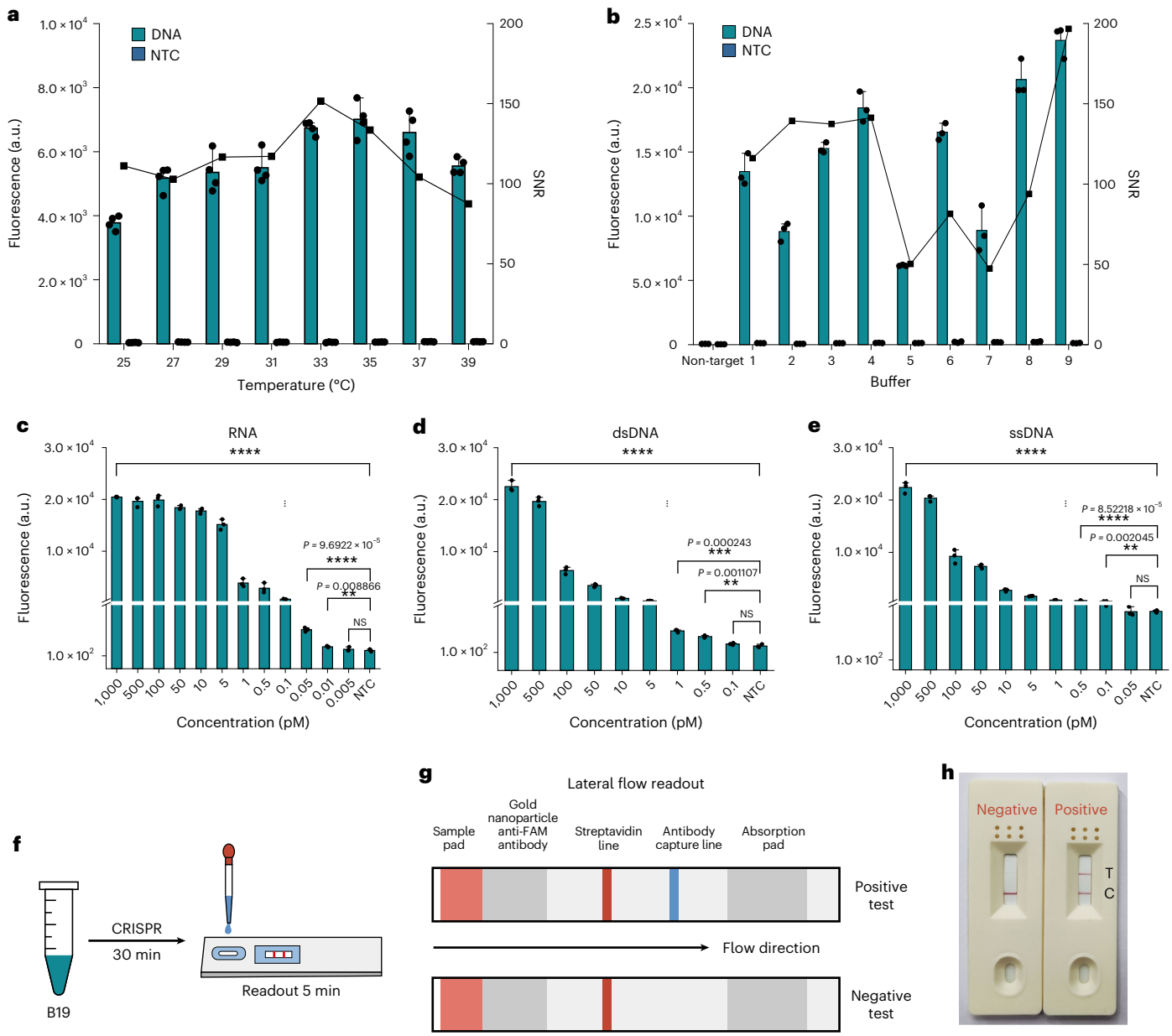

Fig. 3 | Detecting B19 using SUREST. a, Temperature optimization of SURET. The target concentration was 1 nM. $n = 4$ technical replicates; the bars represent the mean ± s.d. **b**, Buffer optimization of SURET. The target concentration was 1 nM. $n = 3$ technical replicates; the bars represent the mean ± s.d. **c**–**e**, Sensitivity analysis for RNA (**c**), dsDNA (**d**) and ssDNA (**e**) detection using LbuCas13a, with concentrations ranging from 0.005 to 1,000 pM. $n = 3$ technical replicates; two-tailed Student's *t*-test. $^{**}P < 0.01$, $^{***}P < 0.001$, $^{****}P < 0.0001$; the bars represent the mean ± s.d. **f**, Depiction of B19 virus detection using SURET integrated with the lateral flow methodology. **g**, The lateral flow readout. **h**, Evaluation of mimic B19 virus samples using lateral flow dipstick strips. Images were captured 5 min after loading the CRISPR reaction mixture.

SURET offers advantages in reagent use and fidelity due to the absence of a T7 transcription step.

To target dsDNA, high temperatures are typically required to suppress interference from the RPA system, which complicates the development of POCT equipment. To overcome this limitation and establish an isothermal detection system, we used RPA with phosphorothioate-containing primers to protect one strand from exonuclease degradation. Upon addition of T7 exonuclease, the unmodified strand was degraded, leaving ssDNA substrates that could be detected by LbuCas13a (Fig. 4c). We chose HBV[35], which causes cirrhosis, liver failure and hepatocellular carcinoma, to test our design. SURET successfully detected HBV mimic targets as low as 10 aM within 25 min under isothermal conditions (37 °C) (Fig. 4d).

To validate our method, we collected 17 clinical samples. Using a threshold set at four times the non-target control (NTC) signal variation, we identified 13 samples as positive and four samples as negative (Fig. 4e), corresponding with the results from quantitative PCR (qPCR) (Fig. 4f). These results demonstrate SURET's capability for field-deployable detection.

Single-nucleotide specificity of SURET

To evaluate SURET's capability in distinguishing single-nucleotide mismatches, we tested fully complementary RNA, dsDNA and ssDNA targets (Supplementary Tables 1, 2 and 4) with single-nucleotide mismatches at several positions (4–28) at a concentration of 1 nM (Fig. 5a). Notably, LbuCas13a targeting RNA (Supplementary Fig. 18a) showed

https://doi.org/10.1038/s41551-025-01424-6

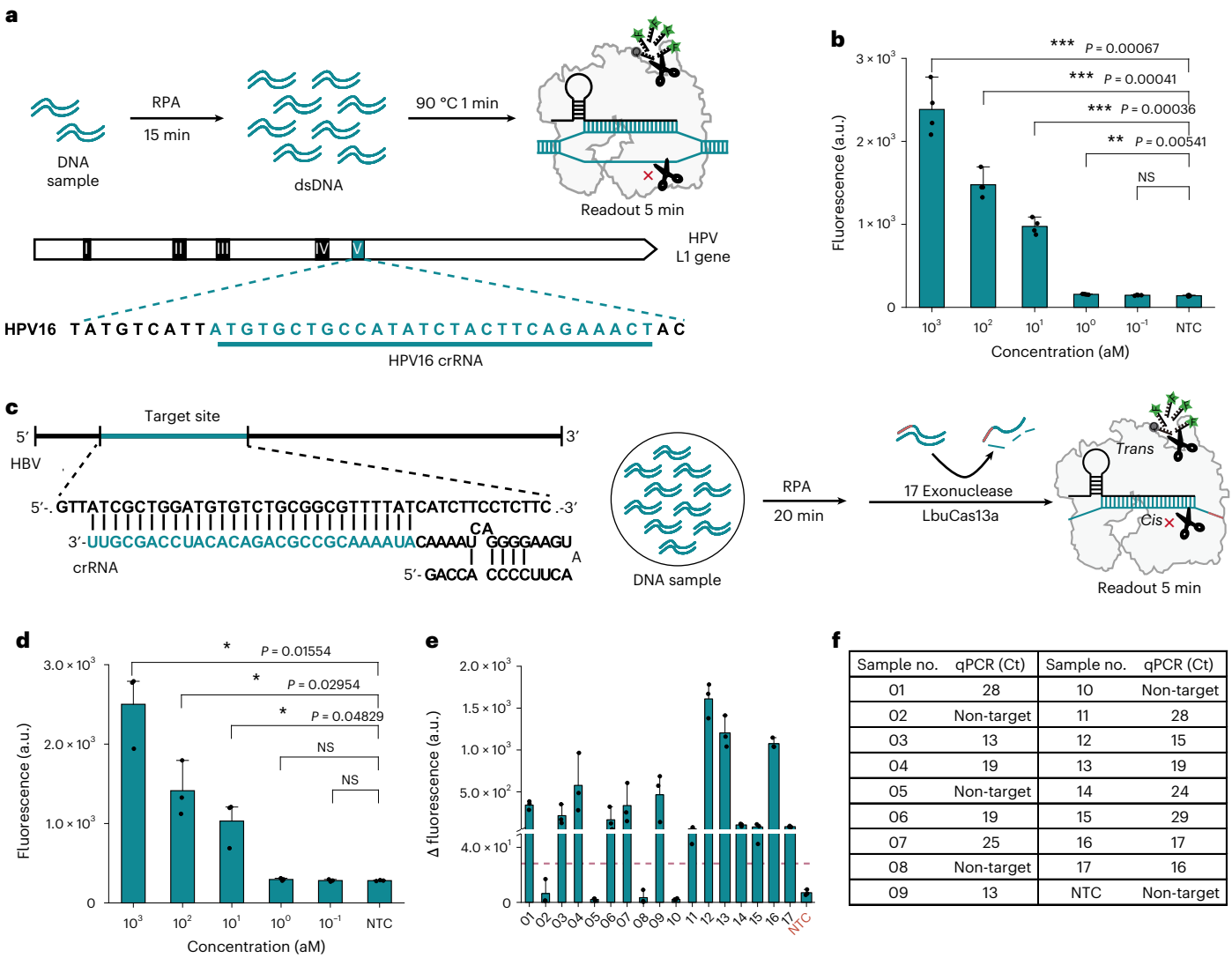

f

Sample no.	qPCR (Ct)	Sample no.	qPCR (Ct)
01	28	10	Non-target
02	Non-target	11	28
03	13	12	15
04	19	13	19
05	Non-target	14	24
06	19	15	29
07	25	16	17
08	Non-target	17	16
09	13	NTC	Non-target

Fig. 4 | SURREST for rapid HPV and hepatitis B virus (HBV) detection. **a**, Schematic representation of the SURREST methodology for mimicking HPV16 (dsDNA) detection, highlighting crRNA (black) and the DNA target site (cyan). **b**, Sensitivity analysis for mimicking HPV16 (dsDNA) detection via LbuCas13a, augmented with RPA. $n = 4$ technical replicates; two-tailed Student's t-test. $^{**}P < 0.01$, $^{***}P < 0.001$; the bars represent the mean ± s.d. **c**, Schematic representation of SURREST for isothermal HBV detection, highlighting the DNA target site (cyan). **d**, Sensitivity analysis for mimicking HBV (dsDNA) detection via LbuCas13a, augmented with RPA. $n = 3$ technical replicates; two-tailed Student's t-test. $^{*}P < 0.05$; the bars represent the mean ± s.d. **e**, HBV clinical sample detection using SURREST. The threshold was set with a fourfold NTC signal variation. $n = 3$ technical replicates; the bars represent the mean ± s.d. **f**, Detection in the HBV clinical samples using qPCR.

little difference in signal between WT and single-nucleotide mismatch, suggesting a lack of single-nucleotide specificity, which is slightly divergent from previous studies indicating minor signal variations between WT and single-nucleotide mismatch[7]. A kinetic analysis (Supplementary Fig. 18b) suggested that the rapid reaction rate in RNA targeting precludes single-nucleotide mismatch specificity. Upon reducing the RNA target concentration to 100 pM, LbuCas13a displayed single-nucleotide specificity predominantly within the seed region (positions 12–20), with peak specificity at position 16 (Fig. 5b). Intriguingly, certain positions (24 and 28) unexpectedly enhanced the *trans*-cleavage activity of complementary RNA, aligning with prior research[36]. Anticipating enhanced specificity in DNA targeting because of weaker crRNA–DNA affinity compared to crRNA–RNA[21], our results confirmed this hypothesis. LbuCas13a targeting DNA exhibited single-nucleotide mismatch specificity, especially for positions 4–20, extending the seed region range relative to RNA targeting, with peak specificity shifting from position 16 to 8 (Fig. 5c,d). This may be attributed to LbuCas13a residues interacting directly only with the base pair at position 8 (ref. 25) and the DNA–RNA duplex reducing this interaction. Additionally, dsDNA targeting revealed high specificity from positions 4 to 20, except for position 12. Closer inspection from positions 8 to 16 indicated higher tolerance for single-nucleotide mismatches at positions 12 and 14 (Supplementary Fig. 19), possibly because of fewer interacting residues at these positions[25]. The highest DF was 12 for dsDNA and 98 for ssDNA, compared to just 5.2 for RNA. Structural studies of LbuCas13a suggested two influential factors: the weaker binding of crRNA to DNA than to RNA[25] and RNA's superior binding to LbuCas13a protein compared to DNA targets[37]. This leads to a weaker affinity between ssDNA targets and the LbuCas13a–crRNA complex, resulting in enhanced single-nucleotide specificity[23]. In summary, these findings demonstrate that single-nucleotide specificity of LbuCas13a in DNA detection is substantially higher compared to RNA detection.

In a comparative analysis, we examined the single-nucleotide specificity of LbuCas13a in ssDNA detection against LbCas12a. While LbCas12a exhibited high specificity for dsDNA, it showed limited capacity for ssDNA detection[9,38]. A slight decrease in signal was

https://doi.org/10.1038/s41551-025-01424-6

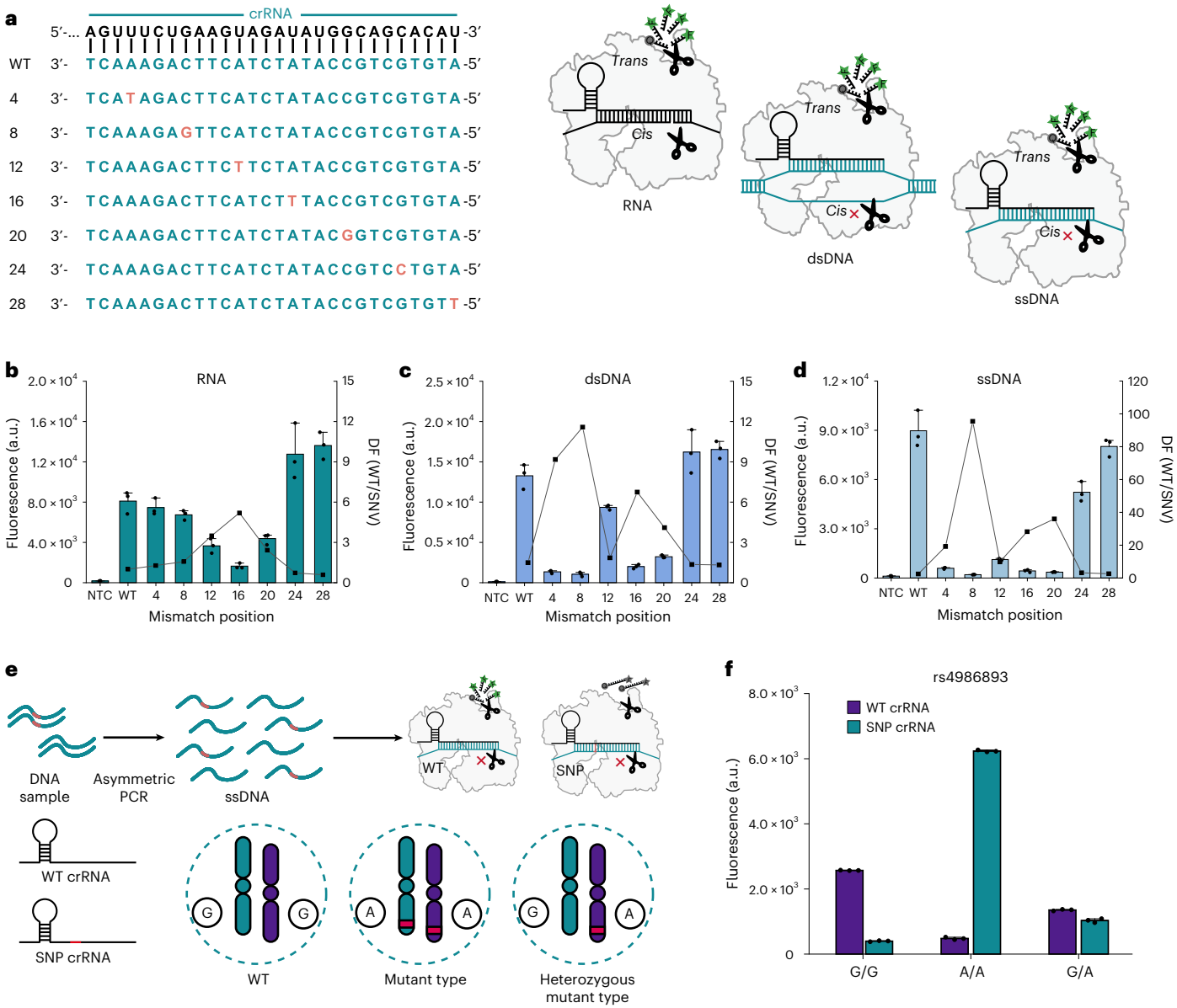

Fig. 5 | Exploring the single-nucleotide specificity of SUREST. a, Schematic diagram of the single-nucleotide mismatched position, highlighting mismatched nucleotides. The crRNA sequence is depicted in black, the DNA target in cyan and the mismatched nucleotide in red. **b**, Analysis of the single-nucleotide specificity of LbuCas13a when targeting RNA. The target concentration was 100 pM. **c**, Evaluation of single-nucleotide specificity in the context of LbuCas13a targeting dsDNA. The target concentration was 1 nM. **d**, Assessment of single-nucleotide specificity during the interaction of LbuCas13a with ssDNA. The target concentration was 1 nM. **e**, Schematic detailing SUREST's application in SNP discrimination, with the SNP locus highlighted in red. **f**, Results of CPY2C19 (rs4986893) using SUREST. $n = 3$ technical replicates; the bars represent the mean ± s.d.

observed for single-nucleotide mismatches between positions 12 and 16 (Supplementary Fig. 20), indicating insufficient specificity for single-nucleotide mismatch detection. In contrast, LbuCas13a targeting ssDNA demonstrated approximately tenfold higher specificity than LbCas12a (Supplementary Fig. 21).

The high single-nucleotide specificity makes SUREST a suitable tool for rapid human genotyping. In this study, we choose CPY2C19 (rs4986893) as a model to test the genotyping ability of SUREST. Combined with asymmetric PCR, SUREST can detect rs4986893 as low as 0.3 aM (0.18 cps μl^{-1}) and reliably discriminate between WT, heterozygous mutant type and mutant type (Supplementary Fig. 22). As shown in Fig. 5e, two different crRNAs were used: WT crRNA, which was fully complementary to the WT sequence, and SNP crRNA, which was fully complementary to the SNP sequence. To determine the genotypes of individuals, we conducted experiments using template plasmid samples. The three genotypes observed in the population included WT, heterozygous mutant type and homozygous mutant type. First, we optimized the asymmetric PCR by screening the primer and primer ratio (Supplementary Fig. 23); then, we selected the best efficiency primer for the following detection (Supplementary Table 2). By using the two crRNAs, we successfully distinguished between the three genotypes, as demonstrated in Fig. 5f. The detection kinetic curves of the different genotypes are shown in Supplementary Fig. 24; G/G, A/A and G/A were easily discriminated once the CRISPR–Cas reaction started. Moreover, we collected kinetic curve data at 5 min to calculate the WT:SNP signal ratio for genotyping rs4986893 (Supplementary Fig. 25). This ratio allowed for a clearer differentiation between the three genotypes, further enhancing the accuracy of the genotyping analysis. Overall,

https://doi.org/10.1038/s41551-025-01424-6

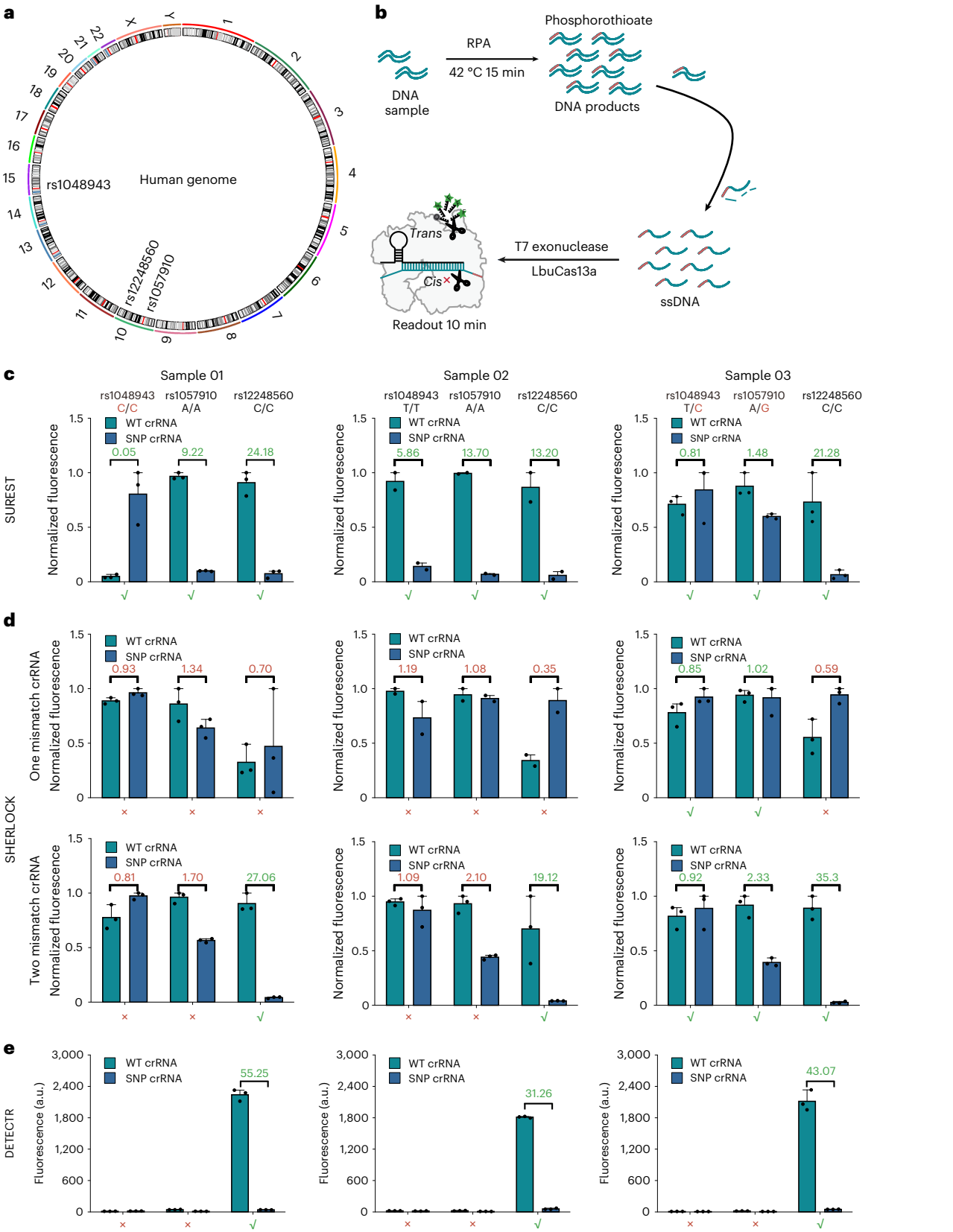

Fig. 6 | SURREST can discriminate SNPs for human genotyping. a, Circos plot showing the location of human SNPs detected using SUREST. **b**, The SUREST mechanism for human genotyping. We used DF to discriminate between WT (DF > 4), heterozygous mutant type (0.25 < DF < 4) and mutant type (DF < 0.25). **c**, SUREST correctly genotyped three different individuals at three different SNP sites in the human genome. **d**, Detection of three different individuals at three different SNP sites in the human genome using SHERLOCK, with one and two mismatch crRNAs. **e**, Detection of three different individuals at three different SNP sites in the human genome using DETECTR. $n = 3$ technical replicates; the bars represent the mean ± s.d. The mutant nucleotide is shown in red; the ticks and crosses indicate the detection results and their correspondence with Sanger sequencing.

the SUREST assay, combined with specific crRNAs, was effective in accurately genotyping rs4986893, enabling the distinction of different genotypes with clarity and precision.

SUREST for human genotyping

To validate the practical application of SUREST in human genotyping, we selected CYP1A1 (rs1048943), CYP2C9 (rs1057910) and rs12248560 representing a range of health-related SNPs (Fig. 6a and Supplementary Table 5). We benchmarked SUREST detection against genotyping data obtained from Sanger sequencing, which served as the gold standard for these SNPs.

Asymmetric PCR demonstrated stable performance (Fig. 5f); however, it requires a thermocycling-capable instrument and is incompatible with one-pot CRISPR–Cas systems because of temperature conflicts. To simplify the detection process for rapid human genotyping, we used RPA with T7 exonucleases instead of asymmetric PCR to generate ssDNA, enabling high single-nucleotide specificity recognition (Fig. 6b). This approach completes human genotyping in 25 min. Additionally, we established a standard for discriminating WT (DF > 4), heterozygous mutant type (0.25 < DF < 4) and mutant type (DF < 0.25) using DF values.

We collected whole-blood samples from ten individuals (two WT, two heterozygous mutant type and six mutant type for rs1048943; nine WT and one heterozygous mutant type for rs1057910; and ten WT for rs12248560, as confirmed by Sanger sequencing) to test SUREST. SUREST demonstrated more than a fivefold signal difference between WT and mutant type, and a within twofold difference for heterozygous mutant type, allowing clear genotype classification (Fig. 6c, Supplementary Fig. 26 and Supplementary Table 6). SUREST accurately identified two WT, two heterozygous mutant type and six mutant type for rs1048943; nine WT and one heterozygous mutant type for rs1057910; and ten WT for rs12248560 among the samples, showing 100% consistency with Sanger sequencing.

We then selected three typical whole-blood samples (sample 01 contained two WT and a mutant type; sample 02 contained three WT; and sample 03 contained two heterozygous mutant types and one WT) to test SHERLOCK and DETECTR. SHERLOCK failed to distinguish WT, heterozygous mutant type and mutant type at these loci without introducing synthetic mismatches in crRNA (Fig. 6d); DF values for all genotypes ranged from 0.3 to 1.5, making identification difficult. Furthermore, SHERLOCK only performed well for rs12248560 and could not genotype rs1048943 and rs1057910, even with synthetic mismatches in crRNA. Similarly, DETECTR only performed well for rs12248560 and showed almost no signal response for rs1048943 and rs1057910 because of the lack of an efficient PAM sequence (Fig. 6e). Detailed detection results from Sanger sequencing, SUREST, SHERLOCK and DETECTR are shown in Supplementary Table 6.

To assess SUREST's ability to detect low-frequency variants, we tested a series of mixture samples (WT and SNV) of rs4986893, which contained SNVs ranging from 0.01% to 100%, with a total concentration of 20 fM. The results, shown in Supplementary Fig. 27, indicate that SUREST demonstrated a signal response with just 0.1% mutations, showing its potential in diagnosing low-frequency mutation samples. The entire SUREST process can be completed in 40 min (30 min for RPA and 10 min for T7 exonuclease degradation with CRISPR–Cas), which is obviously faster than SHERLOCK (over 2 h).

SUREST for genotyping severe acute respiratory syndrome coronavirus 2

To improve genotyping specificity, RNA substrates were amplified using a phosphorothioate-containing primer, while protecting one strand from degradation by exonucleases. The addition of T7 exonuclease degraded the unmodified strand, leaving ssDNA substrates detectable using LbuCas13a (Fig. 7a). To assess the ability of SUREST in RNA virus genotyping, we first used a crRNA targeting the conserved sequence of the N gene to confirm the presence of severe acute respiratory syndrome coronavirus 2 (SARS-CoV-2). Then, three specific mutation sites in the S gene were selected to identify the SARS-CoV-2 variant: K417N for Beta; S477N and T478K for Delta; and Q498R, N501Y and Y505H for Omicron (Fig. 7b). Notably, Omicron also has the K417N mutation, resulting in three signal responses (N gene, K417N, and Q498R, N501Y and Y505H) compared to only two for Beta (N gene and K417N).

We evaluated detection with SUREST using RNA samples from 17 SARS-CoV-2$^+$ and three SARS-CoV-2$^-$ patients (Fig. 7c). Our assay reliably detected SARS-CoV-2 in 20 clinical samples: 17 positive and three negative, as confirmed using qPCR with reverse transcription (RT–qPCR) (Fig. 7g). Furthermore, SUREST accurately distinguished the virus genotypes by using three crRNAs targeting specific mutation sites: six WT; five Beta; three Delta; and three Omicron (Fig. 7d–f), which were confirmed using Sanger sequencing (Supplementary Table 7).

To streamline and reduce the cost of viral extraction and purification, we tested the interference of lysis buffer composition in SUREST. Clinical samples were heated at 95 °C for 5 min with an equal volume of lysis buffer. The results in Supplementary Fig. 28 indicate that lysis buffer composition barely influenced the reaction. Thus, SUREST can reliably distinguish virus genotypes within 30 min. These results indicate that SUREST, with a 30-min workflow from raw sample to virus genotyping, offers a simplified process compared to minimally instrumented SHERLOCK (60 min)[39], SHINE (50 min)[40] and STOPCovid (67 min)[41], and provides a comparable detection time to ITP-CRISPR (30 min)[42] and CRISPR-SPADE (30 min)[43].

Discussion

In the realm of CRISPR-Dx methodologies, Cas13a-based nucleic acid detection platforms stand out for their high sensitivity and rapid response capabilities. Using techniques like RPA[44], loop-mediated isothermal amplification[45] or rolling circle transcription[46], innovative platforms such as CARMEN–Cas13 (ref. 47), DISCoVER[48] and EXTRA-CRISPR[49] have been developed, proving instrumental in diagnosing pathogenic and genetic diseases. This has spurred a surge in research aimed at unravelling the properties and mechanisms of Cas13a through structural biology, paving the way for its broader application in RNA detection and imaging. Traditionally recognized as an RNA-guided and RNA-targeting CRISPR effector, further studies have shed light on the mechanisms of Cas13a in target RNA recognition and cleavage. Dual activation mode responsive to both DNA and RNA targets has been found in Cas12a[50], Cas14a1 (ref. 51) and Cas3 (ref. 52), yet certain aspects of the functionality of Cas13a remain elusive.

Our study uncovered the ability of LbuCas13a to directly target DNA. Supplementary Fig. 29 shows that NTC generates a high signal when a crRNA of LbuCas13a is synthesized through T7 transcription but forgetting to remove the DNA template. Intrigued by this anomaly, we hypothesized that LbuCas13a could directly engage with ssDNA and initiate the *trans*-cleavage activity. To test this, we designed another crRNA (targeting the N gene of COVID-19) produced using chemical synthesis and the corresponding target ssDNA to confirm our hypothesis (Supplementary Fig. 30). As hypothesized, the LbuCas13a–crRNA–ssDNA ternary complex exhibited significant *trans*-cleavage activity upon DNA targeting. This DNA-activated *trans*-cleavage activity was predominantly observed with LbuCas13a, in contrast to the commonly used *Leptotrichia wadei* Cas13a, which exhibited minimal activity (Supplementary Fig. 6). This finding potentially explains why Cas13a has long been categorized solely as an RNA-targeting protein.

Previous studies indicated that Cas9 and Cas12a rely on PAM recognition to initiate unwinding of the protospacer segment in the dsDNA target, thus facilitating subsequent guide RNA invasion and R-loop formation[53,54]. Recently, researchers revealed that DNA topology regulates the interaction between AtCas9 and target DNA, enabling near-PAM-less cleavage[55]. This may provide a possible explanation for LbuCas13a targeting dsDNA. This versatility not only enhances our

https://doi.org/10.1038/s41551-025-01424-6

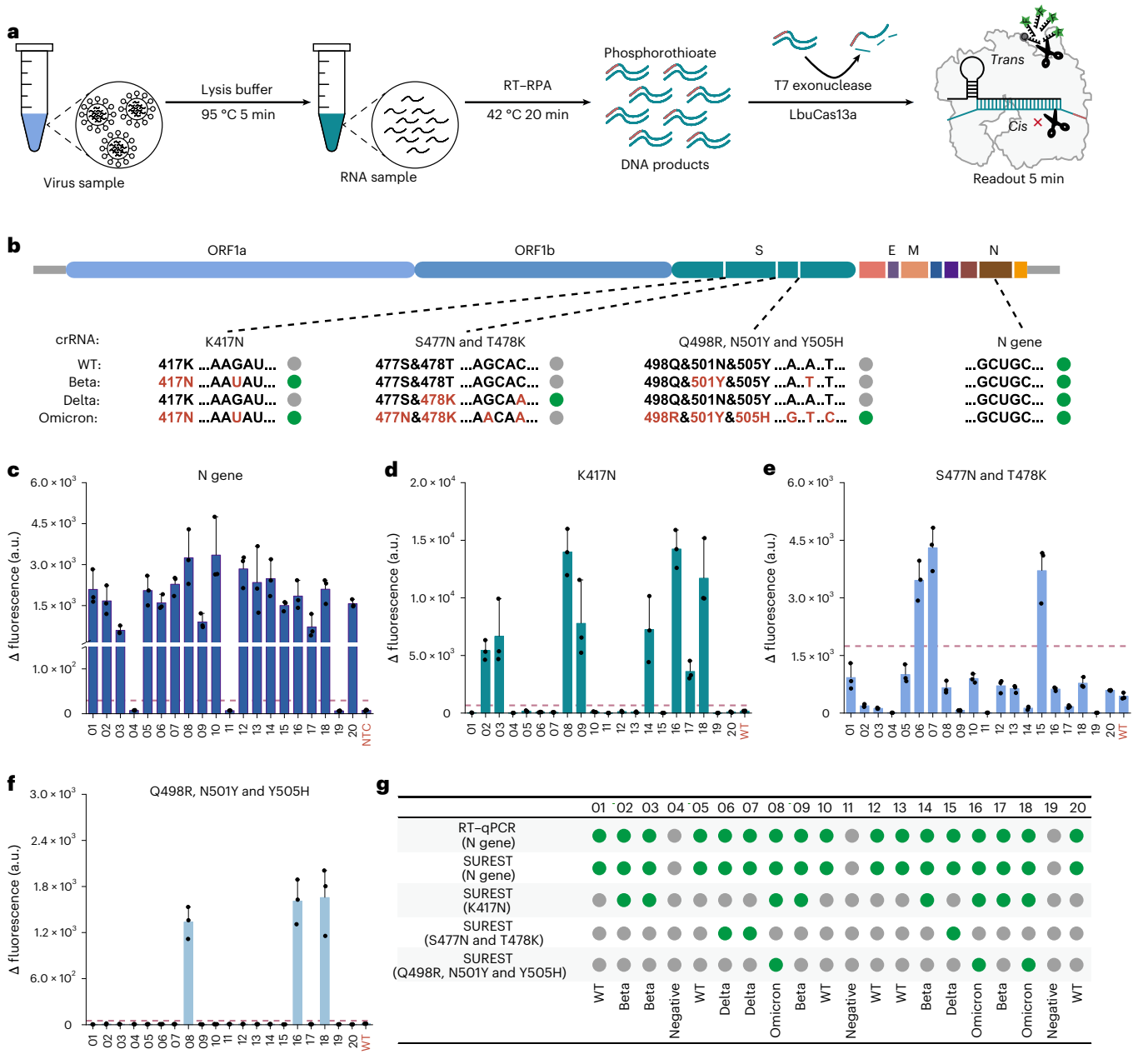

Fig. 7 | SUREST and the genotyping of SARS-CoV-2. a, Schematic of SUREST for the POCT detection of SARS-CoV-2. **b**, Sequences of the N gene, and the K417N, S477N, T478K, Q498R, N501Y and Y505H mutations. **c**, SARS-CoV-2 clinical sample detection using SUREST with N gene crRNA. The threshold was set with a fourfold NTC signal variation. **d**, SARS-CoV-2 clinical sample detection using SUREST with K417N crRNA. The threshold was set with a fourfold WT signal variation. **e**, SARS-CoV-2 clinical sample detection using SUREST with S477N and T478K crRNA. The threshold was set with a fourfold WT signal variation. **f**, SARS-CoV-2 clinical sample detection using SUREST with Q498R, N501Y and Y505H crRNA. The threshold was set with a fourfold WT signal variation. **g**, Detection results of SARS-CoV-2 with RT–qPCR and SUREST. $n = 3$ technical replicates; the bars represent the mean ± s.d. ORF, open reading frame.

grasp of the regulatory mechanisms of the CRISPR–Cas13 system, but also broadens its applicability in molecular diagnostics and imaging. Another intriguing observation pertains to the signal disparity between DNA targets synthesized via T7 transcription, which is entirely complementary to crRNA, and shorter targets matching only the spacer region of crRNA. The anti-tag pairing complementarity effect[56] sheds light on this phenomenon, which was corroborated by our subsequent experiments (Supplementary Fig. 31).

Furthermore, we observed that while DNA targets generate weaker signals compared to RNA targets, their single-nucleotide specificity is remarkably higher. This discrepancy is possibly due to the inherent structural differences between the LbuCas13a–crRNA–RNA and LbuCas13a–crRNA–DNA complexes. Previous studies showed that Cas13a has two conserved higher eukaryotes and prokaryotes nucleotide-binding (HEPN) domains[25], which catalyse crRNA maturation and RNA-guided RNA degradation interdependently using two separated catalytic sites. They observed notable conformational changes that occur upon target RNA binding: the helical-2 domain rotates away from the HEPN2 domain, while the HEPN1 domain rotates towards the HEPN2 domain. In addition, the conformation of crRNA and target is also a key factor in the activation of *trans*-cleavage activity in a CRISPR system[25]. Consequently, and analogous with Cas9, we hypothesize that the difference in conformation between crRNA–RNA (A form) and crRNA–DNA (nearly A form) leads to the different *trans*-cleavage activity[57]. In other words, the conformation of crRNA–DNA enables the helical-2 and HEPN1 domains to rotate, but not completely, which decreases the

trans-cleavage activity of LbuCas13a. On the other hand, when it comes to DNA targets, an incompletely matched crRNA–DNA conformation makes the LbuCas13a–crRNA–DNA ternary complex unstable. Therefore, single-nucleotide mismatch tolerability is decreased, decreasing the *trans*-cleavage activity. Thus, the single-nucleotide sensitivity of the CRISPR-Dx system based on LbuCas13a improved. This provides a possible explanation why the signal strength generated by the DNA target is inferior to the RNA target, but the single-nucleotide sensitivity is noticeably different. Another abnormal phenomenon is that LbuCas13a displayed higher single-nucleotide specificity when targeting ssDNA than dsDNA. This may be because after binding with dsDNA, LbuCas13a does not damage dsDNA, so the effect of the duplex structure on both sides of the spacer converts the conformation of crRNA–DNA to one similar to crRNA–RNA. It makes the single-nucleotide specificity of LbuCas13a targeting dsDNA behave more closely to that of targeting RNA.

Because of limited resources and methodology, the molecular mechanism of LbuCas13a targeting DNA is unclear. The interaction between the LbuCas13a protein, crRNA and DNA target is complex because they are bioactive biomacromolecules. Further exploration should reveal the molecular recognition mechanism of LbuCas13a targeting DNA or its application beyond CRISPR-Dx. Because of limited resources and methodology, the molecular mechanism underlying the ability of LbuCas13a to target DNA is largely unclear. The interactions between LbuCas13a protein, crRNA and DNA are complex because these are large biomacromolecules with intrinsic bioactivity. While our findings suggest that LbuCas13a can bind DNA and release *trans*-cleavage activity, the exact structural and biochemical bases for this activity need to be investigated further. Understanding the molecular recognition mechanisms, including how LbuCas13a unwinds dsDNA, will be crucial. Additionally, further research could explore the potential of LbuCas13a in applications beyond CRISPR-Dx, such as in gene editing, nucleic acid imaging and other molecular diagnostics. These insights could open up new avenues for using Cas13a in varied biotechnology and therapeutic contexts.

In conclusion, our study introduces the SUREST platform, characterized by higher single-nucleotide specificity, high sensitivity (0.18 cps μl^{-1}) and retesting capability. Such single-nucleotide specificity positions LbuCas13a as a tool in nucleic acid detection, particularly in genotyping scenarios. Unlike conventional CRISPR-Dx systems based on Cas13a, such as SHERLOCK[7], SUREST has the added benefit of detecting nucleic acids without the need for a redundant RNA target conversion process. Compared to the CRISPR-Dx systems based on Cas12a, such as DETECTR[9], SUREST can precisely target DNA without being constrained by the PAM sequence. Its ability to continuously output signals without damaging the target holds promise for applications in living cell imaging, virus tracing and beyond. Future exploration into whether other Cas proteins share the properties of LbuCas13a are anticipated.

Methods

Materials and instruments

The LbuCas13a protein was sourced from Bio-Lifesci. The *Leptotrichia wadei* Cas13a protein was obtained from Novoprotein. The LbCas12a protein was obtained from Tolo Biosciences. The TwistAmp Basic Kit was obtained from TwistDx Limited. The Universal DNA Purification Kit was from obtained from BioMed. The Whole Genome DNA Extraction Kit was obtained from LNJNBIO. The Universal Lateral Flow Assay Kit was obtained from Milenia Biotec. The Cas13a buffer was obtained from Tolo Biosciences. NEBuffer 1.0, NEBuffer 2.0, NEBuffer 2.1, NEBuffer r1.1, NEBuffer r2.1, NEBuffer r3.1 and NEBuffer r4.1 were obtained from New England Biolabs. The Bio-Lifesci buffer was obtained from Bio-Lifesci. The RNA sequences (Supplementary Table 1) were obtained from GenScript Biotech Corporation. The ssDNA sequences (Supplementary Table 2) and RNase inhibitors were obtained from Sangon Biotech. The target gene was built on a pUC57-Simple plasmid (Supplementary Table 3) from Tsingke Biotechnology. The 2× Tsingke Master Mix and ArtiCanCEO SYBR qPCR Mix were obtained from Tsingke Biotechnology. The SYBR Green I dye was obtained from Thermo Fisher Scientific. dsDNA (Supplementary Table 4) was produced using PCR and recycled using polyacrylamide gel electrophoresis (PAGE), then purified using the Universal DNA Purification Kit and quantified through the ultraviolet absorption spectrum. We conducted three independent replicate experiments using a single sample.

DNA extraction was carried out using a PEX48 Nucleic Acid platform (Shenzhen living water POCT). Electrophoresis was carried out using a Bio-Rad Laboratories electrophoresis system. Electropherograms were acquired using a Tanon gel imaging system. Nucleic acid quantification was carried out using a microplate reader (BioTek). Real-time fluorescence was measured using a SLAN-96P Real-Time qPCR system or a LineGene 9600 qPCR system (Bioer).

The mutation data for the SARS-CoV-2 virus are readily accessible through the Global Initiative on Sharing Avian Influenza Data repository. Statistical analysis was performed using Microsoft Excel v.2016. Gen5 was used for the statistical analysis of nucleic acid quantification (Agilent Technologies). Sanger sequencing data were provided by Tsingke Biotech. SLAN v.8.2.2 and LineGene 9660 (Bioer) were used for real-time fluorescence. Gel Imaging System v.4.00 (Tanon) and the Image Lab Touch Software (Bio-Rad Laboratories) were used for the electropherograms.

The SARS-CoV-2 samples that the RNA was extracted from were obtained from the Third People's Hospital of Shenzhen. Whole-blood samples and serum samples from patients infected with HBV were obtained from the Shenzhen University Affiliated South China Hospital (approved by the Ethics Review Committee of Shenzhen University Affiliated South China Hospital, approval no. HNLS20240709001-A).

Preparation for the RPA and RPA reaction with reverse transcription

In the RPA reaction, a 50-µl RPA reaction mixture contained 29.5 µl of primer-free rehydration buffer, 2.4 µl of the forward primer (10 µM), 2.4 µl of the reverse primer (10 µM), 5 µl of the sample, 2.5 µl of MgOAc (280 mM) and 12.2 µl of DNase-free or RNase-free water.

In the RPA reaction with reverse transcription (RT–RPA), the 50-µl RPA reaction mixture contained 29.5 µl of primer-free rehydration buffer, 2.4 µl of forward primer (10 µM), 2.4 µl of reverse primer (10 µM), 5 µl of the sample, 2.5 µl of MgOAc (280 mM), 1 µl of RevertAid Reverse Transcriptase (200 U μl^{-1}), 1 µl of RNase inhibitors and 10.2 µl of DNase-free and RNase-free water.

Preparation for the asymmetric PCR reaction

An optimized 25-µl asymmetric PCR reaction was prepared; it contained 200 nM of restrictive primer, 400 nM of non-restrictive primer, 1 fM of DNA template and 1× Tsingke Master Mix. An initial denaturation step of 2 min at 94 °C was followed by 40 cycles of 94 °C for 15 s, 52 °C (or other specified annealing temperature) for 15 s with fluorescence acquisition, and 72 °C for 15 s.

Preparation for CRISPR–Cas13a reaction

Amplification-free detection or combined with PCR. An optimized 20-µl CRISPR–Cas13a reaction was prepared; it contained 10 nM of Cas13a, 500 nM of the RNA reporter, 1× buffer and 10 nM of crRNA. Then, 18 µl of CRISPR–Cas13a was loaded into the bottom of the tubes; 2 µl of the target (DNA, RNA or PCR product) was loaded on the lids. The target was centrifuged to the bottom of the tubes. Reactions were allowed to proceed for 30 min at 33 °C (unless otherwise indicated) on a qPCR system, with fluorescence kinetics measured every 30 s.

Combined with RPA or RT–RPA. An optimized 20-µl CRISPR–Cas13a reaction was prepared; it contained 10 nM of Cas13a, 500 nM of the RNA reporter, 1× buffer and 10 nM of crRNA. Then, 16 µl of CRISPR–Cas13a

was loaded into the bottom of the tubes and 3 µl of the RPA product was loaded on the lids. The target was centrifuged to the bottom of the tubes. Reactions were allowed to proceed for 30 min at 33 °C (unless otherwise indicated) on a qPCR system, with fluorescence kinetics measured every 30 s.

Preparing the CRISPR–Cas12a reaction

Amplification-free detection. An optimized 20-µl CRISPR–Cas12a reaction was prepared; it contained 10 nM of Cas12a, 500 nM of the RNA reporter, 1× buffer and 10 nM of crRNA. Then, 18 µl of CRISPR–Cas12a was loaded into the bottom of the tubes and 2 µl of the target was loaded on the lids. The target was centrifuged to the bottom of the tubes.

RPA/RT–RPA, T7 exonuclease and LbuCas13a one-pot reaction

A 20-µl one-pot reaction contained 1 µl of Cas13a (200 nM), 1 µl of crRNA (200 nM), 1 µl of the RNA reporter (10 µM), 2 µl of Bio-Lifesci buffer (10×), 1 µl of T7 exonuclease (10 U μl^{-1}), 0.5 µl of RNase inhibitors (50 U ul^{-1}) and 10.5 µl of DNase-free or RNase-free water. The 17-µl mixture was loaded into the bottom of the tubes. The RPA/RT–RPA reaction was prepared as described above; 3 µl of the RPA/RT–RPA mixture was loaded on the lids of the tube at 39 °C for 15 min (RPA) or 42 °C for 20 min (RT–RPA). Then, the target was centrifuged to the bottom of the tubes. Reactions were allowed to proceed for 30 min at 33 °C (unless otherwise indicated) on a qPCR system, with fluorescence kinetics measured every 30 s.

DETECTR

An optimized 20-µl CRISPR–LbCas12a reaction was prepared; it contained 50 nM of LbCas12a, 500 nM of the RNA reporter, 1× buffer and 62.5 nM of crRNA. The 17-µl CRISPR–LbCas12a was loaded into the bottom of the tubes and 3 µl of the RPA product was loaded on the lids. The target was centrifuged to the bottom of the tubes.

SHERLOCK

An optimized 20-µl CRISPR–Cas13a reaction was prepared; it contained 45 nM of LbuCas13a, 500 nM of the RNA reporter, 1× buffer, 22.5 nM of crRNA, 0.5 U μl^{-1} of RNase inhibitor, 0.6 U μl^{-1} of T7 polymerase, 1 mM of ATP, 1 mM of uridine-5′-triphosphate, 1 mM of guanosine-5′-triphosphate and 1 mM of cytidine triphosphate. The 17-µl CRISPR–LbuCas13a was loaded into the bottom of the tubes and 3 µl of the RPA product was loaded on the lids. The target was centrifuged to the bottom of the tubes.

PAGE

The PAGE experiments were performed using 15% polyacrylamide gel in Tris-borate-EDTA buffer at 110 V for 2 h. Then, the gel was immersed into the Tris-borate-EDTA buffer containing SYBR Green II RNA Gel Stain or SYBR Green I DNA Gel Stain for 3 min. The image was captured with a standard ultraviolet radiometer.

EMSA

An optimized 20-µl CRISPR–Cas12a reaction was prepared; it contained 500 nM of LbuCas13a or LbCas12a, 50 nM of crRNA, 25 nM of dsDNA target, 1.25 U μl^{-1} of RNase inhibitors and 1× EMSA buffer (100 mM NaCl, 50 mM Tris-HCl, 100 µg ml^{-1} BSA, pH 7.9, at 25 °C). The crRNA and 5′ FAM-labelled target RNA were incubated with the LbuCas13a or LbCas12a for 45 min at 37 °C. Samples were then resolved by 2% agarose gel (1× Tris base, acetic acid and EDTA buffer). Electrophoresis was run for 20 min at 100 V. Then, electropherograms were acquired using a ChemiDoc MP Imaging System (Bio-Rad Laboratories).

Lateral flow assay

Quenchers modified on reporters were replaced by biotin molecules (FAM-UUUUUU-Biotin). To detect B19, the reporter concentration was decreased to 200 nM to avoid strong background signals; other reagents were unchanged.

The SUREST reactions (20 µl) for the lateral flow assay were first incubated at 33 °C for 25 min and then mixed with 20 µl of HybriDetect assay buffer. After mixing, the reaction liquid was applied to the HybriDetect dipstick and incubated for 5 min. Then, the dipstick was observed with the naked eye.

Magnetic bead extraction and target recycling

After the Cas13a reaction, 200 µl of lysate and a 100-µl suspension of 10 µl magnetic beads were added into the centrifuge tube to extract the samples, vortexed and mixed for 5 s, and stored at room temperature for 15 min (vortexed and mixed three times). Magnetic beads were adsorbed with a magnetic separation frame and the supernatant was discarded. Then, 500 µl of washing solution I was added, the tube was vortexed and the contents were mixed for 5 s. The magnetic beads were adsorbed using a magnetic separation frame for instant centrifugation and the supernatant was discarded. Then, 200 µl of washing solution II was added, the tube was vortexed and the contents were mixed for 5 s. The magnetic beads were adsorbed using a magnetic separation frame for instant centrifugation and the supernatant was discarded. Then, 200 µl of washing solution II was added, the tube was vortexed and the contents were mixed for 5 s. The magnetic beads were adsorbed with a magnetic separator using instant centrifugation; all the liquid was carefully absorbed and dried at room temperature for 3 min to remove any ethanol residue. Finally, 20 µl of eluate was added, gently mixed for 15 s, left at room temperature for 2–3 min and centrifuged immediately. Magnetic beads were adsorbed using a magnetic separator, and the eluate containing nucleic acids was recovered into RNase-free centrifuge tubes for subsequent detection.

SARS-CoV-2 clinical sample collection

Extraction-free viral inactivation and lysis were used to release the nucleic acids in the samples to minimize and streamline the costly experimental steps of viral extraction and purification. In this study, RNA extracted from the SARS-CoV-2 samples was mixed with an equal volume of lysis buffer containing 1 U μl^{-1} of RNase inhibitor, 250 µM of tris(2-chloroethyl) phosphate and 0.02 µg μl^{-1} of Chelex 100 at 95 °C for 5 min to achieve rapid detection. Sanger sequencing was carried by Guangzhou IGE Biotechnology.

HBV clinical sample collection

Serum samples from patients infected with HBV were obtained from the South China Hospital Affiliated to Shenzhen University. DNA extraction was carried by the Shanghai Shenggong Health Medical Laboratory. The extracted DNA sample was analysed using SUREST.

Whole-blood sample collection

Whole-blood samples were obtained from the South China Hospital Affiliated to Shenzhen University. DNA was extracted using the PEX48 Nucleic Acid platform using a Whole Genome DNA Extraction Kit. Then, the extracted DNA was analysed using SUREST. Sanger sequencing was carried by Guangzhou IGE Biotechnology.

Statistical analysis

Two-tailed Student's *t*-tests were calculated as follows:

$$t = \frac{\bar{X}_1 - \bar{X}_2}{\sqrt{\frac{(n_1-1)S_1^2+(n_2-1)S_2^2}{n_1+n_2-2}\left(\frac{1}{n_1}+\frac{1}{n_2}\right)}}$$

where $\bar{X}_1$ and $\bar{X}_2$ are the mean value, S_1^2 and S_2^2 are the sample variance, and n_1 and n_2 are the sample size.

DF is calculated as:

$$\mathrm{DF} = \frac{F_{\mathrm{WT}} - F_{\mathrm{WT_0}}}{F_{\mathrm{SNV}} - F_{\mathrm{SNV_0}}}$$

Where F_{SNV} and F_{WT} are the fluorescence signals generated by the SNV and WT targets, respectively. $F_{\mathrm{WT_0}}$ and $F_{\mathrm{SNV_0}}$ represent the initial fluorescence signals generated by the SNV and WT targets.

Reporting summary

Further information on research design is available in the Nature Portfolio Reporting Summary linked to this article.

Data availability

The data supporting the results of this study are available in the paper and its Supplementary Information. The sequencing raw data are available from the Sequence Read Archive under accession nos. PRJNA1242167 and PRJNA1242195.

References

1. Barrangou, R. et al. CRISPR provides acquired resistance against viruses in prokaryotes. *Science* **315**, 1709–1712 (2007).
2. Garneau, J. E. et al. The CRISPR/Cas bacterial immune system cleaves bacteriophage and plasmid DNA. *Nature* **468**, 67–71 (2010).
3. Feng, W. et al. CRISPR technology incorporating amplification strategies: molecular assays for nucleic acids, proteins, and small molecules. *Chem. Sci.* **12**, 4683–4698 (2021).
4. Weng, Z. Y. et al. CRISPR–Cas biochemistry and CRISPR-based molecular diagnostics. *Angew. Chem. Int. Ed. Engl.* **62**, e202214987 (2023).
5. Abudayyeh, O. O. et al. C2c2 is a single-component programmable RNA-guided RNA-targeting CRISPR effector. *Science* **353**, aaf5573 (2016).
6. Zetsche, B. et al. Cpf1 is a single RNA-guided endonuclease of a class 2 CRISPR–Cas system. *Cell* **163**, 759–771 (2015).
7. Gootenberg, J. S. et al. Nucleic acid detection with CRISPR–Cas13a/C2c2. *Science* **356**, 438–442 (2017).
8. Li, S.-Y. et al. CRISPR–Cas12a-assisted nucleic acid detection. *Cell Discov.* **4**, 20 (2018).
9. Chen, J. S. et al. CRISPR–Cas12a target binding unleashes indiscriminate single-stranded DNase activity. *Science* **360**, 436–439 (2018).
10. Myhrvold, C. et al. Field-deployable viral diagnostics using CRISPR-Cas13. *Science* **360**, 444–448 (2018).
11. Huang, X. M., Zhang, X., Zhu, K., Lin, W. & Ma, W. dsmCRISPR: dual synthetic mismatches CRISPR/Cas12a-based detection of SARS-CoV-2 D614G mutation. *Virus Res.* **304**, 198530 (2021).
12. Wu, X. et al. RatioCRISPR: a ratiometric biochip based on CRISPR/Cas12a for automated and multiplexed detection of heteroplasmic SNPs in mitochondrial DNA. *Biosens. Bioelectron.* **241**, 115676 (2023).
13. Yang, H. et al. Sensitive detection of a single-nucleotide polymorphism in foodborne pathogens using CRISPR/Cas12a-signaling ARMS-PCR. *J. Agric. Food Chem.* **70**, 8451–8457 (2022).
14. Arizti-Sanz, J. et al. Simplified Cas13-based assays for the fast identification of SARS-CoV-2 and its variants. *Nat. Biomed. Eng.* **6**, 932–943 (2022).
15. Patchsung, M. et al. A multiplexed Cas13-based assay with point-of-care attributes for simultaneous COVID-19 diagnosis and variant surveillance. *CRISPR J.* **6**, 99–115 (2023).
16. Kim, H. et al. Enhancement of target specificity of CRISPR–Cas12a by using a chimeric DNA–RNA guide. *Nucleic Acids Res.* **48**, 8601–8616 (2020).
17. Ke, Y. et al. Hairpin-spacer crRNA-enhanced CRISPR/Cas13a system promotes the specificity of single nucleotide polymorphism (SNP) identification. *Adv. Sci.* **8**, 2003611 (2021).
18. Chen, Y. et al. Foldback-crRNA-enhanced CRISPR/Cas13a system (FCECas13a) enables direct detection of ultrashort sncRNA. *Anal. Chem.* **95**, 15606–15613 (2023).
19. Gootenberg, J. S. et al. Multiplexed and portable nucleic acid detection platform with Cas13, Cas12a, and Csm6. *Science* **360**, 439–444 (2018).
20. Shinoda, H. et al. Amplification-free RNA detection with CRISPR–Cas13. *Commun. Biol.* **4**, 476 (2021).
21. Lesnik, E. A. & Freier, S. M. Relative thermodynamic stability of DNA, RNA, and DNA:RNA hybrid duplexes: relationship with base composition and structure. *Biochemistry* **34**, 10807–10815 (1995).
22. Yamano, T. et al. Crystal structure of Cpf1 in complex with guide RNA and target DNA. *Cell* **165**, 949–962 (2016).
23. Zhang, C. et al. The mechanical properties of RNA-DNA hybrid duplex stretched by magnetic tweezers. *Biophys. J.* **116**, 196–204 (2019).
24. Liu, L. et al. Two distant catalytic sites are responsible for C2c2 RNase activities. *Cell* **168**, 121–134 (2017).
25. Liu, L. et al. The molecular architecture for RNA-guided RNA cleavage by Cas13a. *Cell* **170**, 714–726 (2017).
26. Ma, J.-Y. et al. 'RESET' effect: random extending sequences enhance the *trans*-cleavage activity of CRISPR/Cas12a. *Anal. Chem.* **94**, 8050–8057 (2022).
27. O'Connell, M. R. Molecular mechanisms of RNA targeting by Cas13-containing type VI CRISPR–Cas systems. *J. Mol. Biol.* **431**, 66–87 (2019).
28. East-Seletsky, A. et al. Two distinct RNase activities of CRISPR-C2c2 enable guide-RNA processing and RNA detection. *Nature* **538**, 270–273 (2016).
29. Hokynar, K. et al. Detection and differentiation of human parvovirus variants by commercial quantitative real-time PCR tests. *J. Clin. Microbiol.* **42**, 2013–2019 (2004).
30. Kaminski, M. M. et al. A CRISPR-based assay for the detection of opportunistic infections post-transplantation and for the monitoring of transplant rejection. *Nat. Biomed. Eng.* **4**, 601–609 (2020).
31. Zhang, Y. B., Chen, Y., Zhang, Q., Liu, Y. & Zhang, X. An aM-level sensitive cascade CRISPR-Dx system (ASCas) for rapid detection of RNA without pre-amplification. *Biosens. Bioelectron.* **230**, 115248 (2023).
32. Fozouni, P. et al. Amplification-free detection of SARS-CoV-2 with CRISPR-Cas13a and mobile phone microscopy. *Cell* **184**, 323–333 (2021).
33. Liu, T. Y. et al. Accelerated RNA detection using tandem CRISPR nucleases. *Nat. Chem. Biol.* **17**, 982–988 (2021).
34. Lin, C., Franceschi, S. & Clifford, G. M. Human papillomavirus types from infection to cancer in the anus, according to sex and HIV status: a systematic review and meta-analysis. *Lancet Infect. Dis.* **18**, 198–206 (2018).
35. Kania, D. et al. Performance of two real-time PCR assays for hepatitis B virus DNA detection and quantitation. *J. Virol. Methods* **201**, 24–30 (2014).
36. Tambe, A., East-Seletsky, A., Knott, G. J., Doudna, J. A. & O'Connell, M. R. RNA binding and HEPN-nuclease activation are decoupled in CRISPR-Cas13a. *Cell Rep.* **24**, 1025–1036 (2018).
37. Ageely, E. A. et al. Gene editing with CRISPR-Cas12a guides possessing ribose-modified pseudoknot handles. *Nat. Commun.* **12**, 6591 (2021).

38. Li, S.-Y. et al. CRISPR-Cas12a has both *cis*- and *trans*-cleavage activities on single-stranded DNA. *Cell Res.* **28**, 491–493 (2018).
39. de Puig, H. et al. Minimally instrumented SHERLOCK (miSHERLOCK) for CRISPR-based point-of-care diagnosis of SARS-CoV-2 and emerging variants. *Sci. Adv.* **7**, eabh2944 (2021).
40. Arizti-Sanz, J. et al. Streamlined inactivation, amplification, and Cas13-based detection of SARS-CoV-2. *Nat. Commun.* **11**, 5921 (2020).
41. Joung, J. et al. Detection of SARS-CoV-2 with SHERLOCK one-pot testing. *N. Engl. J. Med.* **383**, 1492–1494 (2020).
42. Ramachandran, A. et al. Electric field-driven microfluidics for rapid CRISPR-based diagnostics and its application to detection of SARS-CoV-2. *Proc. Natl Acad. Sci. USA* **117**, 29518–29525 (2020).
43. Nguyen, L. T. et al. A thermostable Cas12b from *Brevibacillus* leverages one-pot discrimination of SARS-CoV-2 variants of concern. *EBioMedicine* **77**, 103926 (2022).
44. Li, J., Macdonald, J. & von Stetten, F. Review: a comprehensive summary of a decade development of the recombinase polymerase amplification. *Analyst* **144**, 31–67 (2019).
45. Moehling, T. J., Choi, G., Dugan, L. C., Salit, M. & Meagher, R. J. LAMP diagnostics at the point-of-care: emerging trends and perspectives for the developer community. *Expert Rev. Mol. Diagn.* **21**, 43–61 (2021).
46. Wang, G., Tian, W., Liu, X., Ren, W. & Liu, C. New CRISPR-derived microRNA sensing mechanism based on Cas12a self-powered and rolling circle transcription-unleashed real-time crRNA recruiting. *Anal. Chem.* **92**, 6702–6708 (2020).
47. Ackerman, C. M. et al. Massively multiplexed nucleic acid detection with Cas13. *Nature* **582**, 277–282 (2020).
48. Chandrasekaran, S. S. et al. Rapid detection of SARS-CoV-2 RNA in saliva via Cas13. *Nat. Biomed. Eng.* **6**, 944–956 (2022).
49. Yan, H. et al. A one-pot isothermal Cas12-based assay for the sensitive detection of microRNAs. *Nat. Biomed. Eng.* **7**, 1583–1601 (2023).
50. Rananaware, S. R. et al. Programmable RNA detection with CRISPR-Cas12a. *Nat. Commun.* **14**, 5409 (2023).
51. Wei, Y. et al. *trans* single-stranded DNA cleavage via CRISPR/Cas14a1 activated by target RNA without destruction. *Angew. Chem. Int. Ed. Engl.* **60**, 24241–24247 (2021).
52. Hu, T. et al. Repurposing Type I-A CRISPR-Cas3 for a robust diagnosis of human papillomavirus (HPV).*Commun. Biol.* **7**, 858 (2024).
53. Swarts, D. C. & Jinek, M. Mechanistic insights into the *cis*- and *trans*-acting DNase activities of Cas12a. *Mol. Cell* **73**, 589–600 (2019).
54. Jiang, F. G. et al. Structures of a CRISPR-Cas9 R-loop complex primed for DNA cleavage. *Science* **351**, 867–871 (2016).
55. Shi, Y.-J. et al. DNA topology regulates PAM-Cas9 interaction and DNA unwinding to enable near-PAMless cleavage by thermophilic Cas9. *Mol. Cell* **82**, 4160–4175 (2022).
56. Wang, B. et al. Structural basis for self-cleavage prevention by tag:anti-tag pairing complementarity in type VI Cas13 CRISPR systems. *Mol. Cell* **81**, 1100–1115 (2021).
57. Chen, J. et al. *Trans*-nuclease activity of Cas9 activated by DNA or RNA target binding. *Nat. Biotechnol.* **43**, 558–568 (2025).

Acknowledgements

This work was supported by the Special Foundation for State Major Research Program of China (no. 2022YFB3207200), the Special Fund Project for Medical Research of Shenzhen Municipality (no. D2401014), the National Natural Science Foundation of China (no. 22104048), the Basic and Applied Basic Research Foundation of Guangdong Province (nos. 2022A1515220211 and 2024A1515011877), the Science, Technology and Innovation Commission of Shenzhen Municipality (nos. 20220812142907001 and JCYJ20240813142810015) and the Shenzhen Key Laboratory of Nano-Biosensing Technology (no. ZDSYS20210112161400001). The clinical samples for this study were provided by the Third People's Hospital of Shenzhen and the Shenzhen University Affiliated South China Hospital. We extend our sincere gratitude to these institutions for their invaluable support of this work.

Author contributions

X.W. and S.L. designed and performed the experiments, analysed the data and prepared the manuscript. Y.L. conceived the project and provided overall supervision. Y.C. designed the experiments and wrote the manuscript, with input from all authors. X.Z. provided experimental input, edited the manuscript and co-supervised this work. C.G. and Y.Z. analysed the recycling experiments. J.Z. helped to design and collect the data for amplification. R.H. and X.Y. designed the lateral flow assay, under the supervision of C.L. and Q.Z. S.Z. designed and performed the EMSA experiments. All authors edited and approved the manuscript.

Competing interests

Y.L., S.L. and X.W. are inventors on a patent application (no. CN116590387B) related to Cas13a protein directly for ssDNA detection. The other authors declare no competing interests.

Additional information

Supplementary information The online version contains supplementary material available at https://doi.org/10.1038/s41551-025-01424-6.

Correspondence and requests for materials should be addressed to Yong Chen, Yizhen Liu or Xueji Zhang.

Peer review information *Nature Biomedical Engineering* thanks the anonymous reviewers for their contribution to the peer review of this work. Peer reviewer reports are available.

nature portfolio

Corresponding author(s): Xueji Zhang
Yizhen Liu
Yong Chen

Last updated by author(s): Mar 26, 2025

Reporting Summary

Nature Portfolio wishes to improve the reproducibility of the work that we publish. This form provides structure for consistency and transparency in reporting. For further information on Nature Portfolio policies, see our Editorial Policies and the Editorial Policy Checklist.

Statistics

For all statistical analyses, confirm that the following items are present in the figure legend, table legend, main text, or Methods section.

n/a	Confirmed	
☐	☒	The exact sample size (*n*) for each experimental group/condition, given as a discrete number and unit of measurement
☐	☒	A statement on whether measurements were taken from distinct samples or whether the same sample was measured repeatedly
☐	☒	The statistical test(s) used AND whether they are one- or two-sided *Only common tests should be described solely by name; describe more complex techniques in the Methods section.*
☒	☐	A description of all covariates tested
☒	☐	A description of any assumptions or corrections, such as tests of normality and adjustment for multiple comparisons
☐	☒	A full description of the statistical parameters including central tendency (e.g. means) or other basic estimates (e.g. regression coefficient) AND variation (e.g. standard deviation) or associated estimates of uncertainty (e.g. confidence intervals)
☐	☒	For null hypothesis testing, the test statistic (e.g. *F*, *t*, *r*) with confidence intervals, effect sizes, degrees of freedom and *P* value noted *Give P values as exact values whenever suitable.*
☒	☐	For Bayesian analysis, information on the choice of priors and Markov chain Monte Carlo settings
☐	☒	For hierarchical and complex designs, identification of the appropriate level for tests and full reporting of outcomes
☒	☐	Estimates of effect sizes (e.g. Cohen's *d*, Pearson's *r*), indicating how they were calculated

Our web collection on statistics for biologists contains articles on many of the points above.

Software and code

Policy information about availability of computer code

Data collection	Sanger sequencing data were provided by Tsingke Biotech. Gen5 was used for Statistical analysis of Nucleic acid quantification (Agilent, California, USA). SLAN v8.2.2 (SLAN, Shanghai, China) and Gene-9660 (Bioer, Hangzhou, China) was used for the real-time fluorescence . Gel Image System v4.00 (Tanon, Shanghai, China) and Image Lab Touch Software (Bio-Rad, Hercules, USA) was used for Electropherograms.
Data analysis	Gen5 was used for Statistical analysis of Nucleic acid quantification (Agilent, California, USA). Excel version 2016 was used for Statistical analysis .The cutoff values were determined by computing the negative samples and subsequently adding three times the standard deviation. Additionally, the error bars were computed based on the standard deviation of the mean over triplicate measurements.

For manuscripts utilizing custom algorithms or software that are central to the research but not yet described in published literature, software must be made available to editors and reviewers. We strongly encourage code deposition in a community repository (e.g. GitHub). See the Nature Portfolio guidelines for submitting code & software for further information.

Data

Policy information about availability of data

All manuscripts must include a data availability statement. This statement should provide the following information, where applicable:

- Accession codes, unique identifiers, or web links for publicly available datasets
- A description of any restrictions on data availability
- For clinical datasets or third party data, please ensure that the statement adheres to our policy

The data supporting the results in this study are available within the paper and its Supplementary Information. The sequencing raw data are available from the Sequence Read Archive (SRA) of NCBI under accession number PRJNA1242167 and PRJNA1242195. Source data are provided with this paper.

Research involving human participants, their data, or biological material

Policy information about studies with human participants or human data. See also policy information about sex, gender (identity/presentation), and sexual orientation and race, ethnicity and racism.

Reporting on sex and gender	Whole blood and HBV samples used in this experiment were provided by the South China Hospital Affiliated to Shenzhen University, and have passed safety ethics. The gender of patients was randomly selected during sample selection.
Reporting on race, ethnicity, or other socially relevant groupings	We didn't classify people into different categories.And the samples obtained in this experiment were all provided by the South China Hospital Affiliated to Shenzhen University, and most of them were from Chinese patients.
Population characteristics	The samples obtained in this experiment were all provided by the South China Hospital Affiliated to Shenzhen University, and most of them were from Chinese patients.All clinical samples were obtained from the Shenzhen Third People's Hospital (Shenzhen, China). Although age and sex information was meticulously recorded, the information was not used in the data analysis included in this work. On the basis of results obtained via qPCR, 13 samples tested positive for HBV, whereas 4 samples tested negative.On the basis of results obtained via RT-qPCR, 17 samples tested positive for SARS-CoV-2, whereas 3 samples tested negative.
Recruitment	This experiment has signed relevant cooperation agreements with the South China Hospital Affiliated to Shenzhen University, and Approved by the Ethics Review Committee of Shenzhen University Affiliated South China Hospital, Approval. No.: HNLS20240709001-A.
Ethics oversight	Human samples from patients with SARS-CoV-2, HBV were obtained from the South China Hospital Affiliated to Shenzhen University, Approved by the Ethics Review Committee of Shenzhen University Affiliated South China Hospital, Approval. No.: HNLS20240709001-A.

Note that full information on the approval of the study protocol must also be provided in the manuscript.

Field-specific reporting

Please select the one below that is the best fit for your research. If you are not sure, read the appropriate sections before making your selection.

☒ Life sciences ☐ Behavioural & social sciences ☐ Ecological, evolutionary & environmental sciences

For a reference copy of the document with all sections, see nature.com/documents/nr-reporting-summary-flat.pdf

Life sciences study design

All studies must disclose on these points even when the disclosure is negative.

Sample size	Experiments with synthetic targets had 2-4 technical replicates. Experiments with patient samples had 1 replicate, owing to sample-volumeconstraints.
Data exclusions	The positive samples should have a signal-to-noise ratio three times higher than that of the negative samples. Otherwise, they will be regarded as invalid.
Replication	Each experiment was done with at least 3 replicates to ensure that the results are reproducible. All attempts at replication were successful, and standard deviations were within the expected ranges.
Randomization	We conducted randomization of experimental replicates by assigning each synthetic simulated sample to a detection group in a random order, ensuring unbiased allocation of detections among the samples utilized in this study.
Blinding	Calling a sample positive or negative is determined mathematically (an over-3-fold standard deviation change in 5 minutes), so blinding was not necessary, as user bias does not affect the determination of sample-positivity calling.

Reporting for specific materials, systems and methods

We require information from authors about some types of materials, experimental systems and methods used in many studies. Here, indicate whether each material, system or method listed is relevant to your study. If you are not sure if a list item applies to your research, read the appropriate section before selecting a response.

Materials & experimental systems

n/a	Involved in the study
☐	☒ Antibodies
☒	☐ Eukaryotic cell lines
☒	☐ Palaeontology and archaeology
☒	☐ Animals and other organisms
☒	☐ Clinical data
☒	☐ Dual use research of concern
☒	☐ Plants

Methods

n/a	Involved in the study
☒	☐ ChIP-seq
☒	☐ Flow cytometry
☒	☐ MRI-based neuroimaging

Antibodies

Antibodies used: Antibodies used in the lateral-flow strips include polyclonal (rabbit) anti-FITC antibody labelled with gold particles. The antibodies were included asparts of the lateral-flow assay kit by Milenia Biotec.

Validation: Validation was performed by the supplier (Milenia Biotec).

Plants

Seed stocks: *Report on the source of all seed stocks or other plant material used. If applicable, state the seed stock centre and catalogue number. If plant specimens were collected from the field, describe the collection location, date and sampling procedures.*

Novel plant genotypes: *Describe the methods by which all novel plant genotypes were produced. This includes those generated by transgenic approaches, gene editing, chemical/radiation-based mutagenesis and hybridization. For transgenic lines, describe the transformation method, the number of independent lines analyzed and the generation upon which experiments were performed. For gene-edited lines, describe the editor used, the endogenous sequence targeted for editing, the targeting guide RNA sequence (if applicable) and how the editor was applied.*

Authentication: *Describe any authentication procedures for each seed stock used or novel genotype generated. Describe any experiments used to assess the effect of a mutation and, where applicable, how potential secondary effects (e.g. second site T-DNA insertions, mosiacism, off-target gene editing) were examined.*